

Early Events in the Nonadiabatic Relaxation Dynamics of 4-(*N,N*-Dimethylamino)benzonitrile

Michał A. Kochman,^{*,†} Attila Tajti,[‡] Carole A. Morrison,[§] and R. J. Dwayne Miller[†]

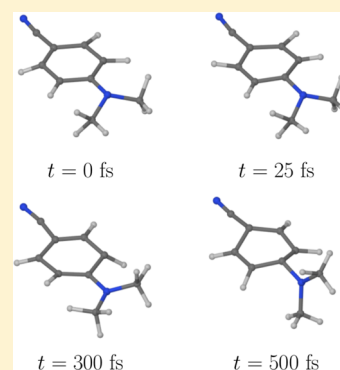
[†]Max Planck Institute for the Structure and Dynamics of Matter, Building 99 (CFEL), Luruper Chaussee 149, 22761 Hamburg, Hamburg, Germany

[‡]Institute of Chemistry, Eötvös Loránd University, Budapest 1053, Hungary

[§]School of Chemistry, University of Edinburgh, Joseph Black Building, David Brewster Road, Edinburgh, Scotland EH9 3FJ

S Supporting Information

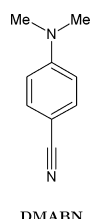
ABSTRACT: 4-(*N,N*-Dimethylamino)benzonitrile (DMABN) is the archetypal system for dual fluorescence. Several past studies, both experimental and theoretical, have examined the mechanism of its relaxation in the gas phase following photoexcitation to the S_2 state, without converging to a single description. In this contribution, we report first-principles simulations of the early events involved in this process performed using the nonadiabatic trajectory surface hopping (TSH) approach in combination with the ADC(2) electronic structure method. ADC(2) is verified to reproduce the ground- and excited-state structures of DMABN in reasonably close agreement with previous theoretical benchmarks. The TSH simulations predict that internal conversion from the S_2 state to the S_1 takes place as early as 8.5 fs, on average, after the initial photoexcitation, and with no significant torsion of the dimethylamino group relative to the aromatic ring. As evidenced by supporting EOM-CCSD calculations, the population transfer from S_2 to S_1 can be attributed to the skeletal deformation modes of the aromatic ring and the stretching of the ring-dimethylamino nitrogen bond. The non- or slightly twisted locally excited structure is the predominant product of the internal conversion, and the twisted intramolecular charge transfer structure is formed through equilibration with the locally excited structure with no change of adiabatic state. These findings point toward a new interpretation of data from previous time-resolved experiments.



1. BACKGROUND

The compound 4-(*N,N*-dimethylamino)benzonitrile (DMABN, Scheme 1) is well-known for its dual fluorescence: on excitation

Scheme 1



by near UV radiation in polar solvents, it exhibits two fluorescence bands, of which one (the “normal” fluorescence) has the usual small Stokes shift, and the “anomalous” other band is strongly red-shifted.¹ The former band is generally assigned to a so-called locally excited (LE) state, while the latter is ascribed to a highly polar intramolecular charge-transfer (ICT) state. The underlying mechanism of this phenomenon, and especially the structure of the ICT state or states, has historically been - and, in some respects, continues to be - the subject of substantial controversy.^{2–17} Because *ab initio* calculations are typically performed in vacuum, the natural starting point for theoretical examination is the photochemistry

of DMABN in the gas phase, rather than in solution. The picture of the relaxation dynamics in the gas phase following photoexcitation to the S_2 state that emerges from experimental studies^{18–21} and high-level calculations^{9,22–25} can be summarized as follows.

In the ground electronic state, the dimethylamino group of the DMABN molecule is slightly pyramidalized and lies roughly in the plane of the aromatic ring. Adopting the terminology of Robb and co-workers,²⁴ in which the nuclear geometry is prefixed with a label denoting the electronic state on which it exists, we will refer to the ground-state structure as S_0 -GS. The dynamics of DMABN in the gas phase after photoexcitation to the S_2 state is shown schematically in Figure 1. Following the initial photoexcitation, the molecule rapidly (in under 100 fs¹⁹) relaxes to reach an S_2/S_1 conical intersection (CI) seam, where it undergoes radiationless decay to the S_1 state. At the S_2/S_1 CI seam, the reaction path branches off into two channels that lead to two distinct structures associated with potential energy minima on the S_1 surface. The first is the near-planar S_1 -LE structure, whose dipole moment is similar in magnitude to²⁴ or somewhat higher²³ than that of S_0 -GS. The second is the ICT structure, for which high-level *ab initio* calculations^{9,23,24} consistently predict a twisted geometry in which the

Received: November 26, 2014

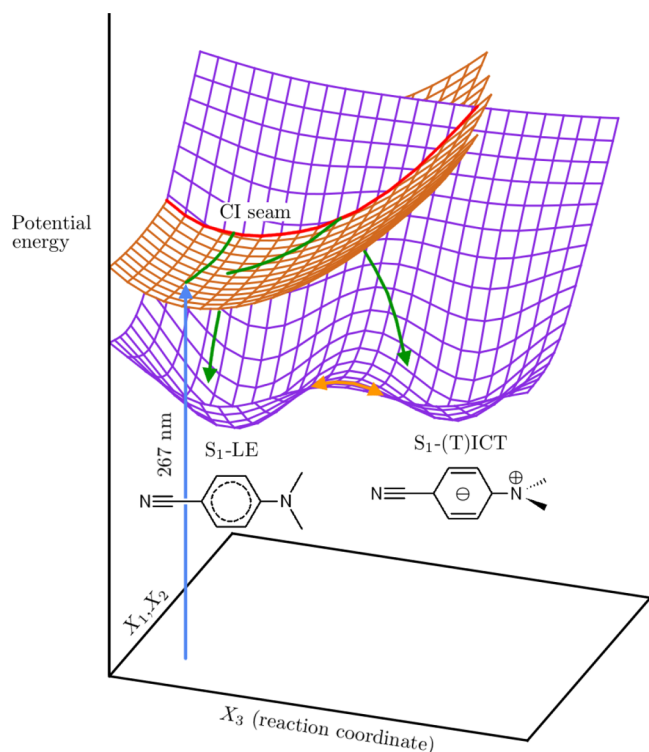


Figure 1. Schematic illustration of the relaxation dynamics of DMABN in the gas phase following photoexcitation to the S_2 state. Note that the topologies of the underlying potential energy surfaces and the CI seam are matters of controversy (see accompanying text for details), and the present diagram represents the view of Robb et al.,²⁴ namely that the S_2/S_1 CI seam lies roughly parallel to the dimethylamino twist coordinate. X_1 and X_2 are the branching space coordinates, which lift the degeneracy at the S_2/S_1 CI seam. The reaction coordinate X_3 mainly involves the dimethylamino group torsion. The ground-state potential energy surface is not shown. Two possible trajectories are visualized as green arrows. In one, the S_2/S_1 CI seam is reached at a nontwisted geometry, and the molecule subsequently relaxes to the S_1 -LE structure, while in the other, the molecule encounters the CI seam at a partially twisted geometry and afterward relaxes to the S_1 -(T)ICT structure. The adiabatic equilibration between S_1 -LE and S_1 -(T)ICT is indicated as an orange arrow.

dimethylamino group is rotated by around 90° relative to the plane of the aromatic ring, and a significantly higher dipole moment than that of S_0 -GS. Hence, it is labeled the S_1 -(T)ICT structure.

There are conflicting views in the literature regarding the molecular geometry on reaching the S_2/S_1 CI seam. According to Robb and co-workers,²⁴ who characterized its topology through calculations at the complete active space self-consistent field (CASSCF) level, the CI seam runs roughly parallel to the dimethylamino group torsional coordinate, and it may be reached at a large range of torsion angles, leading to either of the S_1 -LE and S_1 -(T)ICT structures directly after the internal conversion at the CI seam. The formation of the S_1 -LE structure is favored because the dimethylamino group is not twisted both at the Franck–Condon geometry and at the lowest-energy point on the S_2/S_1 CI seam. The branching space coordinates (denoted X_1 and X_2 in Figure 1) involve skeletal deformations of the aromatic ring and stretching of the N1–C4 bond (see Figure 2 (a) for atom numbering) but not the twisting of the dimethylamino group.

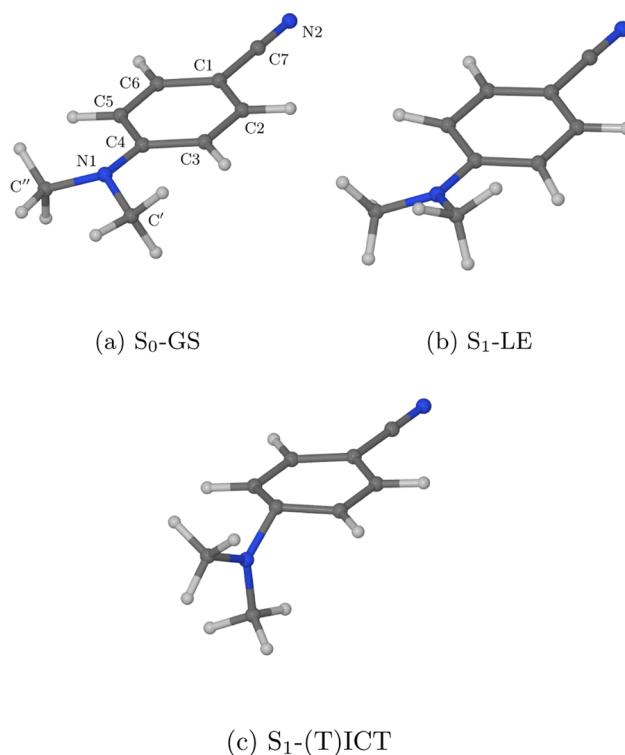


Figure 2. Equilibrium geometries of the S_0 -GS, S_1 -LE, and S_1 -(T)ICT structures of DMABN as optimized at the MP2/ADC(2)/cc-pVDZ level of theory.

This view is contested by the femtosecond time-resolved experimental studies of Fuß et al.,^{19–21} who postulate that the CI seam is preferentially reached at a substantially twisted geometry and that the S_1 -(T)ICT structure is the majority product of the internal conversion process. The same authors also conclude that the branching space does include the torsional coordinate of the dimethylamino group. It should be noted that the theoretically expected location of the lowest-energy point on the CI seam is highly sensitive to the level of theory: using a reduced CASSCF active space, Amatatsu²⁶ located the lowest-energy point on the CI seam at a fully twisted geometry, while Zhang and co-workers,²⁷ also employing CASSCF with a small active space, predicted that the crossing occurs at a partially twisted geometry.

Once the molecule is on the S_1 surface, the S_1 -LE and S_1 -(T)ICT structures equilibrate with each other with no change of adiabatic state (hence this process is commonly referred to as the adiabatic equilibration between the two structures) on a time scale of 1 ps.¹⁹ In the gas phase, the S_1 -(T)ICT structure is somewhat higher in energy than the S_1 -LE, and under experimental conditions (DMABN in the gas phase preheated to 130°C and photoexcited at 276 nm) the equilibrium S_1 -LE/ S_1 -(T)ICT population ratio has been estimated at around 2.¹⁹

Despite the status of DMABN as the archetypal dual fluorescence system, and the considerable amount of theoretical attention it has received, there are only relatively few reports of computer simulations of its excited-state relaxation dynamics. Some such studies^{28–33} focused on the solvation of the photoexcited DMABN molecule, and others^{34,35} used simplified models of the molecule as test cases for the development of simulation methods. In order to improve the theoretical understanding of this important system by providing information that cannot be obtained from static calculations

alone, and may be directly compared to experimental measurements, such as the sequence and time scale of events, we have carried out dynamical (which is to say, time-resolved) simulations of the gas-phase relaxation mechanism. In particular, the present study was intended to resolve the above-mentioned controversy as to whether the S_2/S_1 CI seam is predominantly reached at a twisted or a nontwisted geometry. The relaxation dynamics of photoexcited DMABN involves nonadiabatic transitions between excited electronic states, and in our study these were taken into account through the trajectory surface hopping (TSH) method of Tully and Preston.^{36,37} The electronic structure of DMABN was treated using the second-order algebraic-diagrammatic construction³⁸ (ADC(2)) method, which provides a satisfactorily realistic description of the electronic structure of its excited states at a moderate computational cost.

The rest of the paper is organized as follows. First, we briefly review the TSH method and define the simulation parameters. We then critically discuss the performance of the ADC(2) method for the ground- and excited-state structures of DMABN. Finally, we present the results of the TSH simulations and analyze them in the context of the available experimental and theoretical data.

2. COMPUTATIONAL METHODS

2.1. The Trajectory Surface Hopping Method. In the TSH method, the nuclear wavepacket of the system is represented by a so-called ‘swarm,’ or ensemble, of mutually independent semiclassical trajectories. Within each trajectory, the nuclei are described using classical mechanics, while the electrons are treated quantum-mechanically. The time-dependent wave function $\Phi(\mathbf{r}, t)$ of the electrons is written as a linear combination of adiabatic electronic wave functions $\phi_j(\mathbf{r}; \mathbf{R})$:

$$\Phi(\mathbf{r}, t) = \sum_j a_j(t) \phi_j(\mathbf{r}; \mathbf{R}) \exp\left[-\frac{i}{\hbar} \int E_j(\mathbf{R}) dt\right] \quad (1)$$

Here, $\mathbf{R} = \mathbf{R}(t)$ denotes a classical trajectory followed by the nuclei. \mathbf{r} is the position vector of the electrons, and the adiabatic electronic wave functions $\phi_j(\mathbf{r}; \mathbf{R})$ are the solutions of the time-independent, “clamped-nuclei” electronic Schrödinger equation, $\hat{H}_{\text{el}}(\mathbf{r}, \mathbf{R}) \phi_j(\mathbf{r}; \mathbf{R}) = E_j(\mathbf{R}) \phi_j(\mathbf{r}; \mathbf{R})$. The requirement that $\Phi(\mathbf{r}, t)$ satisfies the time-dependent electronic Schrödinger equation

$$\hat{H}_{\text{el}}(\mathbf{r}, \mathbf{R}) \Phi(\mathbf{r}, t) = i\hbar \frac{\partial}{\partial t} \Phi(\mathbf{r}, t) \quad (2)$$

leads to the following set of coupled differential equations for the time-evolution of the expansion coefficients $a_i(t)$

$$\dot{a}_i = - \sum_j a_j C_{ij} \exp\left[-\frac{i}{\hbar} \int (E_j - E_i) dt\right] \quad (3)$$

where $C_{ij} = \langle \phi_i | (\partial/\partial t) | \phi_j \rangle$ is the nonadiabatic coupling element (NACME) between states i and j . The square modulus $f_j(t) = |a_j(t)|^2$ of the expansion coefficient of state j can be interpreted as the population of that state at time t . One furthermore defines nonadiabatic coupling vectors (NACVs) between pairs of states i and j as $\mathbf{d}_{ij} = \langle \phi_i | \nabla | \phi_j \rangle$, where ∇ denotes the gradient with respect to the nuclear coordinates. The NACMEs are related to the NACVs by

$$C_{ij} = \sum_A \mathbf{v}_A \cdot \mathbf{d}_{ij,A} \quad (4)$$

where \mathbf{v}_A is the velocity of nucleus A , and $\mathbf{d}_{ij,A}$ denotes the component of \mathbf{d}_{ij} corresponding to that nucleus.

Within each simulated trajectory, at any time the system is considered to exist in some current adiabatic state k from among the states which appear in the expansion (1). The nuclear dynamics are propagated according to Newton’s equations of motion on the potential energy surface of that state:

$$\ddot{\mathbf{R}}_A = -\frac{1}{M_A} \nabla_A E_k(\mathbf{R}) \quad (5)$$

Here, ∇_A denotes the gradient with respect to the Cartesian coordinates of nucleus A . The total energy of the system is taken as the sum of the energy E_k of the current state and the kinetic energy T of all atoms. Nonadiabatic effects are accounted for by allowing the system to undergo a switch (or “hop”) between the current state and another adiabatic state, which then becomes the new current state. In the variant of the TSH method used in the present work, a hop is allowed to occur at each step of the nuclear dynamics, and the hopping probability is calculated by means of the fewest switches criterion of Tully,³⁹ which aims to ensure that the fraction of the total number of trajectories evolving on any state j is proportional to its population $f_j(t) = |a_j(t)|^2$ averaged over all trajectories, while minimizing the total number of hops per trajectory. For example, in the case of a two-state system, Tully’s fewest switches criterion takes on a particularly simple mathematical form: at every time step of duration Δt , the probability P_{kj} of a hop from the current state k to the other state j is

$$P_{kj} = \max\left(\frac{\dot{f}_j}{f_k} \Delta t, 0\right) \quad (6)$$

At every time step, P_{kj} is compared with a random number ζ distributed uniformly in the range $(0, 1)$, and a hop from k to j is imposed if $\zeta < P_{kj}$. Whenever a hop does occur, the nuclear momenta must be rescaled in such a way as to maintain the energy conservation of the system. In the implementation of the TSH method used in the present work, the nuclear momenta are rescaled uniformly according to

$$\mathbf{p}^{(1)} = \mathbf{p}^{(0)} \sqrt{\frac{T^{(0)} + (E_k - E_j)}{T^{(0)}}} \quad (7)$$

where the superscripts $^{(0)}$ and $^{(1)}$ denote quantities before and after the hop, respectively.

2.2. MP2/ADC(2) Calculations. Previous work by Köhn and Hättig²³ has shown that the second-order approximate coupled-cluster (CC2) method correctly describes the two lowest electronic states of DMABN and the equilibrium geometries of the S_1 -LE and S_1 -(T)ICT structures. However, the well-documented propensity of the CC2 method for convergence problems in the vicinity of intersections between excited electronic states^{40–42} makes it ill-suited for the purpose of nonadiabatic molecular dynamics simulations, and we have instead elected to use the closely related ADC(2)^{38,45,46} method, which does not suffer from that problem.

Ground-state MP2^{43,44} and excited-state ADC(2) calculations were performed within the computational chemistry

software package Turbomole version 6.3.1,⁴⁷ taking advantage of frozen core and resolution of the identity approximations. For the sake of brevity, in what follows we will often collectively refer to both these electronic structure methods as MP2/ADC(2). Unless otherwise noted, the MP2/ADC(2) calculations were carried out using the cc-pVDZ⁴⁸ basis set in combination with the default auxiliary basis set for cc-pVDZ.⁴⁹

The equilibrium geometries of the ground- and excited-state structures S_0 -GS, S_1 -LE, and S_1 -(T)ICT were optimized at the MP2/ADC(2) level of theory. The geometry optimizations were performed in Cartesian coordinates with no symmetry constraints, and all resulting structures were confirmed to correspond to potential energy minima by calculating numerically the normal modes of the molecule. Afterward, vertical excitation energies at the S_0 -GS equilibrium geometry to the S_1 and S_2 states were computed. In order to check for basis-set-size effects, the single point energy of each of the structures S_0 -GS, S_1 -LE, and S_1 -(T)ICT as optimized at the MP2/ADC(2) level with the cc-pVDZ basis set was subsequently recalculated with the use of the larger cc-pVTZ basis set, as well as with the aug-cc-pVTZ basis set which additionally includes diffuse basis functions on all atoms.⁴⁸ The corresponding auxiliary basis sets were used.⁴⁹

The TSH simulations aimed to model the relaxation dynamics of DMABN in the gas phase following photo-excitation to the S_2 state. The simulations were carried out with the use of the implementation of the TSH method provided in the software package Newton-X,^{42,50,51} which contains an interface to Turbomole. This implementation relies on two approximations: first, nonadiabatic coupling between excited states is calculated using the finite differences scheme of Hammes-Schiffer and Tully.⁵² Within this approach, the NACME at time t is computed from overlap integrals of adiabatic electronic wave functions i and j at the current and previous time steps:

$$C_{ij}(t) = \frac{1}{4\Delta t} [3\langle\phi_i(t - \Delta t)|\phi_j(t)\rangle - 3\langle\phi_j(t - \Delta t)|\phi_i(t)\rangle - \langle\phi_i(t - 2\Delta t)|\phi_j(t - \Delta t)\rangle + \langle\phi_j(t - 2\Delta t)|\phi_i(t - \Delta t)\rangle] \quad (8)$$

Second, the electronic wave functions that enter the above equation are approximate configuration interaction singles (CIS) wave functions, rather than the actual ADC(2) wave function.

The initial conditions (sets of atomic positions and velocities) for the TSH simulations were sampled from the Wigner quantum harmonic oscillator distribution for the ground state, which was computed using the program initcond.pl from the simulation package Newton-X. Twenty-four trajectories were propagated for a time period of 1.5 ps. The nuclear dynamics was propagated using the velocity Verlet integrator with a time step of 0.5 fs, while the time-evolution of the coefficients $a_i(t)$ was propagated with the default fifth-order integrator of Butcher⁵³ and with a time step of 0.025 fs, using quantities interpolated between the classical time steps. Adiabatic states from S_1 to S_3 were included in the linear expansion (1), and NACMEs were calculated between all pairs of excited states, while the coupling of excited states with the ground state was neglected (assumed to be zero). The initially occupied state was the S_2 state, and its initial population was set to unity.

2.3. Coupled Cluster Calculations. The NACVs d_{ij} , the calculation of which is not available at the MP2/ADC(2) level, play an important role in the theoretical description of nonadiabatic effects. Namely, in both the mean-field⁵⁴ (Ehrenfest) and the TSH methods for the simulation of nonadiabatic dynamics, the NACVs govern the time-evolution of the populations of the adiabatic states through eqs 3 and 4. Equation 4, in particular, reveals the significance of the components $d_{ij,A}$ of the NACV that correspond to individual nuclei: the rapid change of the populations in a region of strong coupling can be conceptually associated with the motions of a subset of nuclei whose components $d_{ij,A}$ of the NACV are large and parallel or antiparallel to their respective velocity vectors \mathbf{v}_A .

Clearly, then, knowing the NACVs between the S_2 and S_1 states of DMABN at the time of the internal conversion from the former state to the latter would improve our understanding of the nuclear motions involved in this process. Accordingly, we have calculated, using the equations-of-motion coupled cluster with single and double excitations (EOM-CCSD) method,⁵⁵ the NACV at the time of the first hop from S_2 to S_1 in each of the simulated trajectories and visually inspected the resulting NACVs. The EOM-CCSD method was selected for this purpose because it is fairly close, in terms of electron correlation treatment, to the MP2/ADC(2) method. (Both methods include dynamic electron correlation but account for static correlation only in excited states.) The EOM-CCSD calculations were performed using a development version of the *ab initio* electronic structure program CFOUR.^{56,57} A restricted Hartree–Fock (RHF) reference determinant was used. The cc-pVDZ basis set⁴⁸ was utilized, and the frozen core approximation was applied. The nonadiabatic coupling vectors were calculated analytically using the method of Tajti and Szalay.⁵⁸

3. RESULTS AND DISCUSSION

3.1. Static Calculations. The equilibrium geometries of the structures S_0 -GS, S_1 -LE, and S_1 -(T)ICT as optimized at the MP2/ADC(2)/cc-pVDZ level of theory are shown in Figure 2 (a), (b), and (c), respectively, and in Table 1 they are characterized by listing a selection of energetic and geometric quantities. The equilibrium geometries as well as the TSH trajectories were described in terms of a set of parameters whose definitions we will now provide. The twisting of the dimethylamino group was characterized by a quantity ϕ defined as the average of the absolute values of the torsion angles formed by the atoms C'–N1–C4–C3 and C''–N1–C4–C5 (see Figure 2 (a) for atom numbering):

$$\phi = \frac{1}{2} (|\phi(\text{C}'\text{--N1--C4--C3})| + |\phi(\text{C}''\text{--N1--C4--C5})|) \quad (9)$$

In the TSH simulations, the molecule was considered to exist in the S_1 -LE structure if it was occupying the S_1 adiabatic state and the value of ϕ was less than 45° . If, on the other hand, the molecule was occupying the S_1 state and ϕ was in the range from 75° to 105° , it was considered to exist in the S_1 -(T)ICT structure. The pyramidalization of the dimethylamino nitrogen N1 was monitored by calculating the (signed) distance $d(\text{N1})$ between nitrogen N1 and the plane containing the atoms C', C'', and C4. Likewise, for carbon C4, $d(\text{C4})$ was defined as the (signed) distance between C4 and the plane defined by the atoms N1, C3, and C5.

Table 1. Energies (E), Vertical Excitation Energies (ΔE), Magnitudes of Dipole Moment (μ), Bond Lengths (R), and Selected Other Geometric Parameters of the S_0 -GS, S_1 -LE, and S_1 -(T)ICT Structures of DMABN, Calculated Using the MP2 and ADC(2) Methods

level of theory		S_0 -GS	S_1 -LE	S_1 -(T)ICT
MP2/ADC(2)/cc-pVDZ	E , eV ^a	0	3.963	3.765
	$\Delta E(S_1)$, eV ^b	4.495		
	$\Delta E(S_2)$, eV ^b	4.750		
	μ , D	6.7	9.9	13.0
	ϕ , °	17.1	21.0	88.6
	$d(N1)$, Å	0.243	0.108	0.011
	$d(C4)$, Å	0.007	0.017	0.359
	$R(N1-C4)$, Å	1.392	1.400	1.455
	$R(C4-C3)$, Å	1.421	1.422	1.458
	$R(C4-C5)$, Å	1.421	1.422	1.459
	$R(C3-C2)$, Å	1.398	1.450	1.383
	$R(C5-C6)$, Å	1.398	1.450	1.383
	$R(C2-C1)$, Å	1.410	1.421	1.439
	$R(C6-C1)$, Å	1.410	1.421	1.439
MP2/ADC(2)/cc-pVTZ	E , eV ^c	0	3.940	3.836
	$\Delta E(S_1)$, eV ^b	4.389		
	$\Delta E(S_2)$, eV ^b	4.644		
	μ , D	6.7	10.1	13.2
MP2/ADC(2)/aug-cc-pVTZ	E , eV ^c	0	3.880	3.790
	$\Delta E(S_1)$, eV ^b	4.325		
	$\Delta E(S_2)$, eV ^b	4.540		
	μ , D	7.0	10.3	13.4

^aThe energy values are quoted relative to the energy of the S_0 -GS structure and include vibrational zero-point corrections. ^bVertical excitation energies to the S_1 and S_2 states calculated at the S_0 -GS equilibrium geometry. ^cSingle-point energy calculated at the MP2/ADC(2)/cc-pVDZ geometry, and with zero-point corrections obtained at the MP2/ADC(2)/cc-pVDZ level.

In line with previous CASSCF,²⁴ CC2,²³ and DFT⁵⁹ calculations, S_0 -GS is predicted to exhibit a near-planar geometry with a slightly pyramidalized dimethylamino nitrogen, and a quinoid aromatic ring (the bonds C3–C2 and C5–C6 are significantly shorter than the other four bonds in the aromatic ring). The calculated vertical excitation energies to the S_1 and S_2 states, at 4.495 and 4.750 eV, respectively, are both overestimated slightly relative to the respective experimental values of 4.0 and 4.4 eV.⁶ The increase of the basis set size to cc-pVTZ, and the addition of diffuse functions in the aug-cc-pVTZ basis set, each have the effect of decreasing the calculated excitation energies to S_1 and S_2 , but the energy gap between the two states does not change significantly with increasing basis set size. The above suggests that increasing the basis set size stabilizes each of the two excited states relative to the ground state to a similar extent, and so the cc-pVDZ basis set is already sufficient to describe the internal conversion from S_2 to S_1 .

Moving on to discuss the excited-state structures, both S_1 -LE and S_1 -(T)ICT are confirmed to correspond to minima on the S_1 surface. Their equilibrium geometries and electric dipole moments very closely resemble those calculated by Köhn and Hättig²³ at the CC2 level, which is unsurprising given the close relationship of these methods to each other. For S_1 -LE an equilibrium geometry is predicted in which the dimethylamino group is near-planar and slightly twisted relative to the aromatic

ring. The aromatic ring itself is distorted in an antiquinoid manner, which is to say, the bonds C3–C2 and C5–C6 are now markedly longer than the other four bonds. The S_1 -(T)ICT structure, true to its name, features a full twist of the dimethylamino group relative to the aromatic ring and a high dipole moment of 13.0 D. The carbon atom C4 is strongly pyramidalized, while the dimethylamino group is near-planar. The aromatic ring has a quinoid character, with the C3–C2 and C5–C6 bonds being significantly shorter than the other four bonds.

A convenient means to analyze the nature of an excited electronic state is the electron density difference map (EDDM), which is defined simply as the difference of the electron density of the excited state and that of the ground state at the same nuclear geometry. EDDMs for the S_1 and S_2 states of DMABN were generated at each of the S_0 -GS, S_1 -LE, and S_1 -(T)ICT geometries and are shown in Figure 3. It is evident that the EDDM for the S_1 state at the S_0 -GS geometry is very similar in form to the EDDM for the S_1 state at the S_1 -LE geometry: both reveal a transfer of electron density from the dimethylamino group nitrogen atom to the C2, C3, C5, and C6 carbon atoms of the aromatic ring. Hence, the adiabatic S_1 state at the S_0 -GS and S_1 -LE geometries can be identified as the same diabatic state (the L_b -type state; the diabatic states' labels originate from their symmetry properties, which are discussed briefly in the Supporting Information). Moreover, the EDDM for the S_2 state at the S_0 -GS geometry closely resembles that for the S_2 state at the S_1 -LE geometry: both show a shift of electron density from the dimethylamino group nitrogen to the C4 carbon atom of the aromatic ring and, to a lesser extent, to the nitrile group nitrogen. Thus, the adiabatic S_2 state at the S_0 -GS and S_1 -LE geometries corresponds to the same diabatic state (the L_a -type state). It follows that internal conversion from the S_2 adiabatic state to the S_1 state near the ground-state geometry also involves a change of diabatic state from L_a to L_b .

At the S_1 -(T)ICT geometry, in turn, the diabatic character of the S_1 and S_2 states is rather similar: in both states there is a substantial shift of electron density from the dimethylamino group nitrogen onto the carbon atoms of the aromatic ring and especially C4.

In summary, the MP2/ADC(2)/cc-pVDZ model chemistry very closely reproduces previously reported ground- and excited-state equilibrium geometries of S_0 -GS, S_1 -LE, and S_1 -(T)ICT. It does not, however, correctly predict the experimentally observed energy ordering of the two minima on the S_1 surface, as S_1 -(T)ICT is calculated to be lower in energy than S_1 -LE (by 0.198 eV when applied with the cc-pVDZ basis set, taking into account zero-point corrections). This error is not fully remedied by increasing the basis set size to cc-pVTZ or by the addition of diffuse basis functions, which suggests that it is due to a deficiency of the MP2/ADC(2) method itself. Taking as a benchmark Köhn's and Hättig's²³ best theoretical value (obtained at the CC2 level with higher-order corrections from the CCSDR(3) method⁶⁰) for the relative energies of the two structures, according to which S_1 -(T)ICT is higher in energy than S_1 -LE by 0.17 eV, we estimate that the MP2/ADC(2)/cc-pVDZ model chemistry over-stabilizes S_1 -(T)ICT relative to S_1 -LE by 0.37 eV. Since this error is not drastically large, we have nevertheless proceeded to apply the MP2/ADC(2) method in TSH simulations while taking into account the fact that it may unrealistically shift the adiabatic equilibrium between the S_1 -LE and S_1 -(T)ICT structures toward the latter.

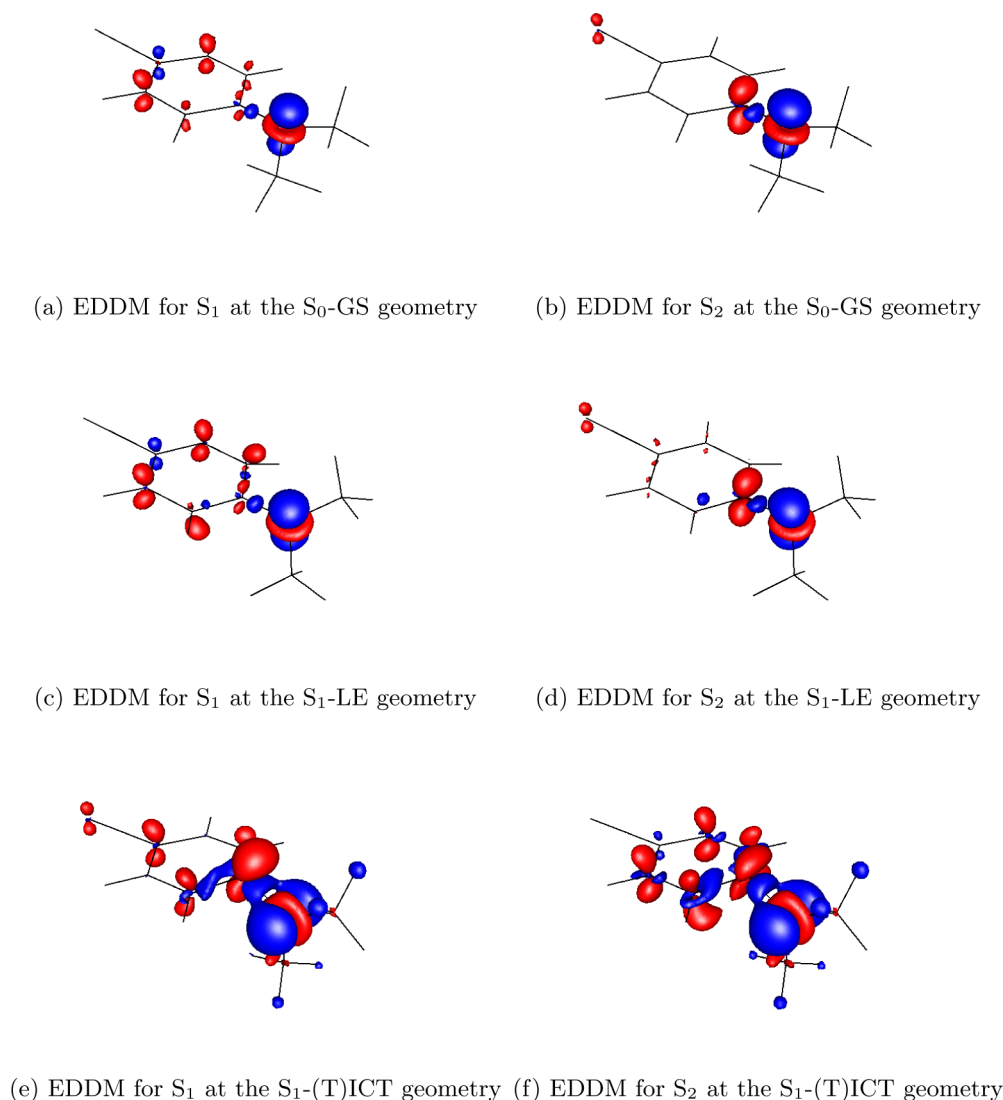


Figure 3. EDDMs for the S_1 and S_2 states of DMABN calculated at the relevant ground- and excited-state geometries, plotted in the form of isosurfaces with an isovalue of $0.01 e/a_0^3$. For each excited state, the red and blue isosurfaces delimit regions in which the electron density is increased and decreased, respectively, relative to the ground state.

The partially twisted intramolecular charge transfer⁹ (S_1 -pTICT) and rehybridized intramolecular charge transfer^{9,24} (S_1 -(R)ICT) structures reported to exist on the S_1 surface at the CASSCF level do not correspond to potential energy minima at the MP2/ADC(2) level. The failure to account for the existence of the S_1 -(R)ICT structure does not invalidate the MP2/ADC(2) method because, in vacuum, the potential energy of that structure is too high for it to be involved in the relaxation mechanism.^{9,24} Regarding, in turn, the S_1 -pTICT structure, the S_1 -LE structure as predicted at the MP2/ADC(2) level (slightly twisted at $\phi = 21.0^\circ$, $\mu = 9.9$ D) appears to have intermediate character between the S_1 -LE (nontwisted, $\mu = 6.5$ D) and S_1 -pTICT (partially twisted at $\phi = 53.4^\circ$, $\mu = 14.4$ D) structures found at the CASSCF level by Coto et al.⁹ Thus, although the S_1 -LE structure predicted by the MP2/ADC(2) method does not coincide closely with either the S_1 -LE or the S_1 -pTICT structure predicted at the CASSCF level, this does not represent a qualitative failure on the part of the MP2/ADC(2) method but rather a fairly minor difference in the topology of the S_1 surface.

3.2. TSH Simulations. We now turn our attention to the TSH simulations, the results of which are summarized in Table 2. Furthermore, the time-evolution of the reaction coordinates ϕ , $d(N1)$, and $d(C4)$ is displayed in Figure 4 (a), (b), and (c), respectively, while the fraction of trajectories evolving in the S_2 and S_1 adiabatic states is plotted in Figure 4 (d). Each of the 24 trajectories followed a broadly similar sequence of events. To accompany this narrative, in the Supporting Information we provide animations of trajectories 1, 2, and 6. At an average of 8.5 fs after the initial photoexcitation, the system underwent a hop from the S_2 adiabatic state to S_1 , while concurrently the population of S_2 decayed to near zero and the population of S_1 increased to near unity. In many trajectories, the S_2 state was later reoccupied temporarily, but after around $t = 300$ fs, all simulated trajectories remained predominantly in the S_1 state. Concurrently with the population transfer from S_2 to S_1 , the dimethylamino nitrogen N1 underwent a subtle change of geometry, switching from the slightly pyramidalized Franck–Condon geometry to a near-planar geometry characteristic of the S_1 -LE structure. The nitrogen N1 subsequently went through umbrella-type inversions around the planar geometry,

Table 2. Breakdown of the Results of the TSH Simulations

trajectory	$t_{\text{hop}}, \text{fs}^a$	$\phi_{\text{hop}}, ^\circ^a$	$t_{\text{TICT}}, \text{fs}^b$
1	7.0	5.4	819.5
2	8.5	25.3	480.5
3	10.5	6.3	333.0
4	5.5	8.9	474.0
5	8.5	9.9	382.5
6	2.0	8.5	304.0
7	13.0	11.5	579.0
8	4.5	15.8	360.0
9	4.5	11.2	397.5
10	8.0	8.3	313.0
11	2.0	16.5	404.0
12	10.5	8.6	468.0
13	24.5	5.2	305.5
14	6.5	8.7	500.0
15	8.0	10.6	196.5
16	2.5	8.8	231.0
17	5.5	5.3	269.0
18	13.0	30.4	268.5
19	13.0	15.5	372.5
20	6.0	15.4	240.5
21	3.0	10.9	355.0
22	26.0	2.6	279.0
23	5.5	11.3	271.5
24	7.0	6.2	310.0

^a t_{hop} is the time at which the system hopped from the S_2 state to the S_1 for the first time, and ϕ_{hop} is the value of the torsional coordinate ϕ at that point. ^b t_{TICT} is the time at which the system reached the S_1 -(T)ICT structure.

which are visible as oscillations around $d(\text{N1}) = 0$ in Figure 4 (b), and which continued for the remainder of the simulated trajectories. The S_3 adiabatic state was never occupied in the simulated trajectories, and its population did not exceed 0.0025 at any time. Hence, we conclude that the S_3 state is not involved in the relaxation mechanism to any significant extent.

In the Supporting Information, we plot the NACME calculated using the approximations mentioned in Section 2.2, and the energy gap, between the S_2 and S_1 states during the initial 300 fs of trajectories 1 to 4. The inspection of these plots shows that the approximate NACME depends on the energy gap in the expected way, in the sense that it adopts large values, positive or negative, when the energy gap is small.

In Figure 5, we present the NACVs between S_2 and S_1 at the time of the first hop from the former state to the latter in trajectories 1 to 4, calculated at the EOM-CCSD/cc-pVDZ level. (The calculated NACVs for all trajectories are also displayed in the Supporting Information.) It can be seen that the NACVs are consistently dominated by in-plane skeletal deformations of the aromatic ring and stretching of the N1–C4 bond. The NACVs do not have large components on the atoms comprising the two methyl groups. Hence, the population transfer from S_2 to S_1 can be associated with the deformations of the aromatic ring and the N1–C4 stretch but not with the torsion of the dimethylamino group. This finding is entirely consistent with the internal conversion mechanism predicted theoretically by Robb and co-workers,²⁴ according to which the branching space at the S_2/S_1 CI comprises the exact same modes.

Within the initial 250 fs period, in all MP2/ADC(2)-based trajectories the dimethylamino group began to undergo a

twisting motion around the N1–C4 bond. In a few trajectories (of which one is indicated in Figure 4 (a) with an arrow), this led to the molecule adopting, temporarily at least, the slightly twisted S_1 -LE structure. In most trajectories, however, the twisting motion continued until the molecule adopted the S_1 -(T)ICT structure on average at around $t = 400$ fs. The carbon atom C4 became pyramidalized as the molecule reached the S_1 -(T)ICT structure and remained so for most of the subsequent trajectory. After reaching the S_1 -(T)ICT structure, the molecule continued to undergo large-amplitude torsional motions around the N1–C4 bond, occasionally returning to the slightly twisted S_1 -LE geometry. This interconversion between S_1 -LE and S_1 -(T)ICT was not accompanied by a change in the adiabatic state of the system, and as such we regard it as the adiabatic equilibration between S_1 -LE and S_1 -(T)ICT. In reality, in the gas phase the S_1 -LE structure is lower in energy than the S_1 -(T)ICT and is the dominant form in the adiabatic equilibrium. The fact that in the TSH simulations, the adiabatic equilibrium is shifted toward the S_1 -(T)ICT structure can be attributed to the overstabilization of that structure by the MP2/ADC(2) method. No instance was observed of the energy gap between the S_1 and S_0 states decreasing to below 0.5 eV, which indicates that thermally activated internal conversion to the ground state (known to be possible from both experimental⁶¹ and theoretical²⁴ studies) is not significant on time scales of the order of 1 ps.

The results outlined above are largely in line with the mechanism of S_2 to S_1 internal conversion as proposed by Robb et al.²⁴ We find that internal conversion from S_2 to S_1 (specifically, the first hop from S_2 to S_1 in the simulated trajectories) invariably took place extremely rapidly after the initial photoexcitation and very close to the nontwisted Franck–Condon geometry. This point deserves special consideration in light of the topology of the S_2/S_1 CI seam. Although the CASSCF calculations of Robb et al.²⁴ predict that the CI seam exists over a wide range of dimethylamino group torsion angles, and may therefore also be accessed over a wide range of torsion angles, they do not necessarily indicate that this possibility is realized. Indeed, as pointed out in the work just cited, the topology of the CI seam indicates that internal conversion at a nontwisted geometry is most likely. The present TSH simulations indicate that the formation of the non- or slightly twisted S_1 -LE is the predominant or even exclusive outcome of the internal conversion step. It follows that internal conversion at a substantially twisted geometry, if it occurs, must be only a minor pathway in the relaxation mechanism. The simulated dynamics subsequently continued on the S_1 surface, and the system entered the stage of adiabatic equilibrium between the slightly twisted S_1 -LE structure and the fully twisted S_1 -(T)ICT structure. The S_1 -(T)ICT structure was populated only through the adiabatic equilibration process.

It should be emphasized that the MP2/ADC(2) method used in the present work provides a significantly different treatment of electron correlation than the CASSCF method employed by Robb et al.²⁴ The former accounts for only dynamical electron correlation, while the latter includes static correlation but typically recovers only a small fraction of the dynamical correlation energy. Thus, the close agreement of both computational approaches regarding the preferred geometry on reaching the S_2/S_1 CI seam cannot be a simulation artifact due to a deficiency shared by both methods.

On the other hand, comparison with the experimental results of Fuß et al.^{19–21} is more problematic, due to the fact that

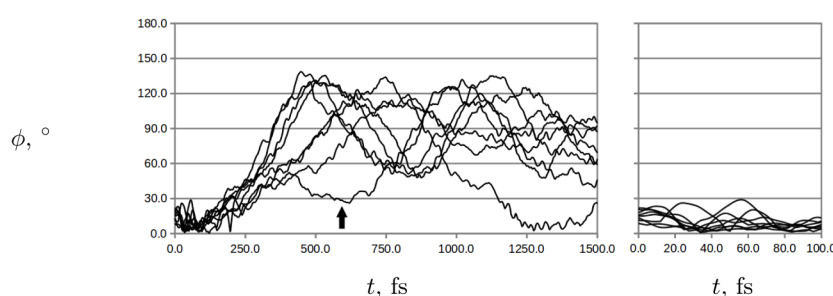
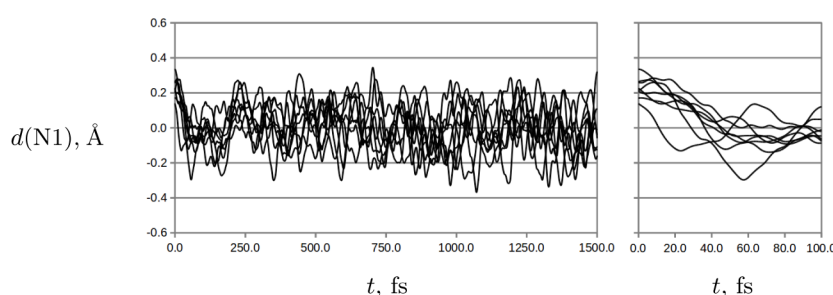
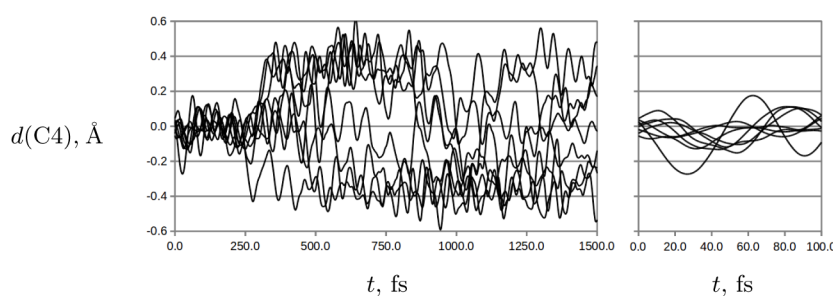
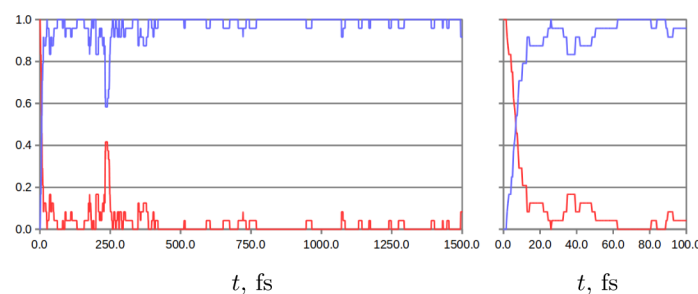
(a) Dimethylamino group torsional coordinate, ϕ (b) Pyramidalization coordinate of nitrogen N1, $d(N1)$ (c) Pyramidalization coordinate of carbon C4, $d(C4)$ (d) Fraction of trajectories evolving in the S_2 and S_1 states

Figure 4. Time-evolution of the reaction coordinates ϕ , $d(N1)$, and $d(C4)$ and the fraction of trajectories proceeding in each adiabatic state along the trajectories simulated using the MP2/ADC(2) method. In order to avoid clutter, the plots (a) to (c) include only trajectories 1 to 8. Analogous plots for trajectories 9 to 24 have been relegated to the Supporting Information. The insets to the right of each plot show the same quantities during the initial 100 fs period of the simulated trajectories.

probing with ionization followed by mass-selective detection yields lifetimes (or, time constants) of locations on the molecular potential energy surfaces, but no direct information on nuclear coordinates, and also because the interpretation of the experimental data relied on the premise that the CI seam is preferentially encountered at a significantly twisted geometry. The lifetime of the location existing immediately after the initial photoexcitation is $\tau_1 = 5 \pm 5$ fs, which was ascribed to the molecule leaving the Franck–Condon region while remaining

in the S_2 state. The duration of τ_1 coincides very closely with the average time of internal conversion (8.5 fs) obtained in our present simulations. It therefore seems reasonable to assume that, in reality, τ_1 corresponds to the lifetime of the molecule in the S_2 state immediately following the initial photoexcitation.

The lifetime of the second location is $\tau_2 = 63 \pm 7$ fs, and it was assigned to the molecule reaching the S_2/S_1 CI seam via a twist of the dimethylamino group. The occurrence of the twist was inferred from the anisotropy of the ion signals. However,

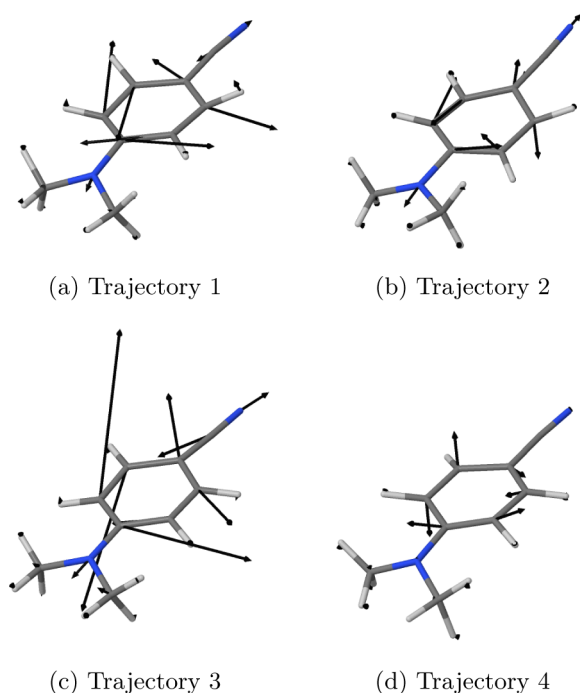


Figure 5. Illustrations of the NACVs between S_2 and S_1 at the time of the first hop from the former state to the latter in trajectories 1 to 4, calculated at the EOM-CCSD/cc-pVDZ level.

the present simulations suggest that the internal conversion process is already under way within a few femtoseconds of the initial photoexcitation and that it occurs at a nontwisted geometry. Possibly, then, τ_2 could arise from the molecule relaxing on the S_1 surface from the nontwisted Franck–Condon geometry to the slightly twisted S_1 -LE.

The validity of this hypothesis hinges on our prediction that the S_1 -LE structure is, in fact, slightly twisted, rather than nontwisted. To the best of our knowledge, no experimental gas-phase study has attempted to distinguish between possible slightly and nontwisted S_1 -LE structures. In the molecular crystal phase, however, a slightly twisted excited-state structure of DMABN has been reported by Techert et al.⁶² Much as in the gas phase, nonexcited DMABN molecules in the molecular crystal phase at room temperature adopt a nontwisted geometry with a slightly pyramidalized dimethylamino group. In the study just cited, DMABN crystals were irradiated at 267 nm, causing the photoexcitation of a fraction of the molecules, and their structures were subsequently analyzed through time-resolved powder X-ray diffraction. To the experimental data, a two-phase model was fitted, in which one phase (p_1) was the original nonexcited phase, and the other phase (p_2) consisted of photoexcited molecules. The fitting parameters included the dimethylamino group torsion and inversion of molecules comprising the photoexcited phase p_2 as well as the occupancy of that phase. The photoexcited molecules were determined to possess an average torsion angle of around 9.5° and a near-planarized dimethylamino group and were found to decay over a period of the order of 1 ns. This small twist is consistent with the formation of the slightly twisted S_1 -LE structure but not with the fully twisted S_1 -(T)ICT structure (the formation of which would have been prevented by the packing of the crystal lattice).

Also, our hypothesis is supported by the observation that the fairly short duration of τ_2 seems in better agreement with a

slight twist leading to the slightly twisted S_1 -LE structure than with a more pronounced twist that would be required for the formation of S_1 -(T)ICT.

The third lifetime of $\tau_3 = 1 \pm 0.3$ ps was attributed to the adiabatic equilibration between S_1 -LE and S_1 -(T)ICT. In agreement with this assignment, in our present simulations the adiabatic equilibration occurs on a time scale of similar order. Further events in the relaxation process, such as intersystem crossing to a triplet state and decomposition, occur over considerably longer periods of time (tens or hundreds of picoseconds) and are not modeled by the present simulation approach.

As a final illustration of the relaxation mechanism predicted at the MP2/ADC(2) level, in Figure 6 we present snapshots of

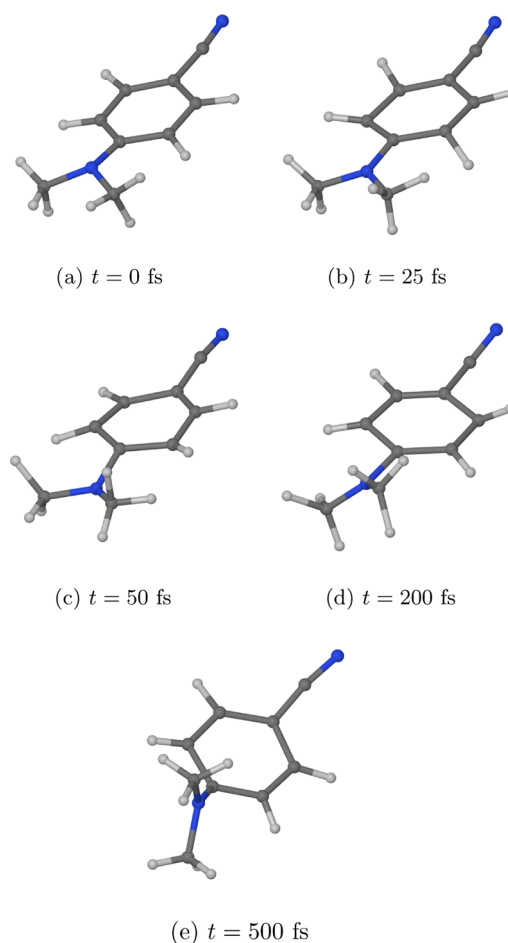


Figure 6. Snapshots of trajectory 6 at selected times during the simulation. The initial photoexcitation takes place at $t = 0$ fs.

the molecule at various times along trajectory 6, which was selected as a representative simulated trajectory. By $t = 25$ fs, the molecule has undergone a hop from S_2 to S_1 and exists in the S_1 -LE structure. The snapshot at $t = 200$ fs shows the molecule undergoing a torsional motion of the dimethylamino group, and by $t = 500$ fs, it has reached the S_1 -(T)ICT structure, in which it remains until the end of the simulation at $t = 1.5$ ps.

Moreover, Figure 7 shows the evolution of the energies of the adiabatic states S_1 and S_2 during the initial stage of trajectory 6. The two states are very close in energy (less than 0.1 eV apart) already at the start of the trajectory; this is a

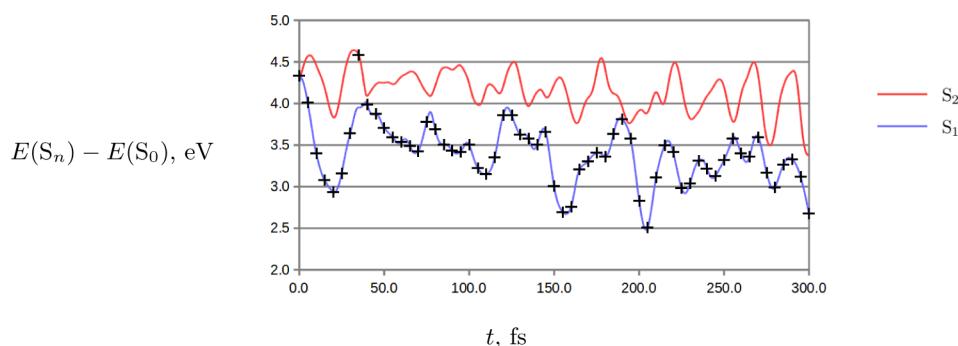


Figure 7. Energies of the adiabatic states S_1 and S_2 during the first 300 fs of trajectory 6. The energies are plotted relative to the energy of the S_0 state, and the currently occupied state is marked with black crosses.

situation which occurs in some, but not all, simulated trajectories. The first hop from S_2 to S_1 takes place within only 2.0 fs of the initial photoexcitation, and the S_2 state is subsequently reoccupied only for a short period of time from $t = 35.0$ to 39.0 fs. Several close avoided crossings occur between the S_1 and S_2 curves during its first 300 fs, which reflects the fact that the S_2/S_1 CI seam is readily accessible near the Franck–Condon geometry.

4. CONCLUSIONS

The relaxation dynamics of DMABN in the gas phase following photoexcitation to the S_2 state was modeled computationally with the use of the TSH method in combination with the MP2/ADC(2) *ab initio* electronic structure method. The MP2/ADC(2) method predicts the relevant excited-state structures of DMABN in good agreement with previous benchmark CASSCF^{9,24} and coupled cluster calculations,²³ except that the S_1 -(T)ICT structure is overstabilized relative to the S_1 -LE.

The results of the TSH simulations reinforce a previous theoretical prediction²⁴ that the internal conversion from S_2 to S_1 state preferentially takes place at a nontwisted geometry and that the non- or slightly twisted S_1 -LE structure is by far the favored outcome. The inspection of the NACVs between S_2 and S_1 shows that it is the skeletal deformation modes of the aromatic ring, and the stretching of the N1–C4 bond, that are responsible for the population transfer from the former state to the latter. The fully twisted S_1 -(T)ICT structure is expected to form mainly through adiabatic equilibration with S_1 -LE. However, this model of the internal conversion process is in conflict with the experimental studies by Fuß et al.,^{19–21} where the internal conversion was instead proposed to occur at a significantly twisted geometry, and at a longer time delay after the initial photoexcitation. This discrepancy may possibly be reconciled through a reinterpretation of the experimentally observed time constants in the light of the results of the TSH simulations. Further investigations, and in particular experimental studies employing methods that directly probe atomic motions, are clearly needed in order to decisively resolve the sequence of events in the initial few hundred femtoseconds after photoexcitation.

■ ASSOCIATED CONTENT

Supporting Information

Cartesian coordinates of the S_0 -GS, S_1 -LE, and S_1 -(T)ICT equilibrium geometries of DMABN as optimized at the MP2/ADC(2)/cc-pVDZ level of theory. A brief discussion of the symmetry properties of the relevant excited electronic states of

DMABN. Plots of the reaction coordinates ϕ , $d(N1)$, and $d(C4)$ for trajectories 9 to 24. Visualizations of NACVs between S_2 and S_1 at the time of the first hop from the former state to the latter in simulated trajectories, calculated at the EOM-CCSD/cc-pVDZ level. Plots of the approximate NACME and the energy gap between the S_2 and S_1 states during the initial 300 fs of trajectories 1 to 4. Animations of selected simulated trajectories. This material is available free of charge via the Internet at <http://pubs.acs.org>.

■ AUTHOR INFORMATION

Corresponding Author

*E-mail: michal.kochman@mpsd.mpg.de.

Notes

The authors declare no competing financial interest.

■ ACKNOWLEDGMENTS

We wish to thank Dr. Rachel Crespo-Otero and Dr. Felix Plasser for helpful discussions on the simulation program Newton-X. Attila Tajti gratefully acknowledges financial support by Orszagos Tudomanyos Kutatasi Alap (OTKA; Grant No. 104672). This work made use of the EaSTCHEM Research Computing Facility (<http://www.chem.ed.ac.uk/content/research-computing-facility>) and the Edinburgh Compute and Data Facility (ECDF) (<http://www.ecdf.ed.ac.uk/>).

■ REFERENCES

- (1) Lippert, E.; Lüder, W.; Moll, F.; Nägele, W.; Boos, H.; Prigge, H.; Seybold-Blankenstein, I. *Angew. Chem.* **1961**, 73, 695–706.
- (2) Grabowski, Z. R.; Rotkiewicz, K.; Rettig, W. *Chem. Rev.* **2003**, 103, 3899–4031.
- (3) Parusel, A. B. J.; Rettig, W.; Sudholt, W. *J. Phys. Chem. A* **2002**, 106, 804–815.
- (4) Rotkiewicz, K.; Grellmann, K. H.; Grabowski, Z. R. *Chem. Phys. Lett.* **1973**, 19, 315–318.
- (5) Grabowski, Z. R.; Rotkiewicz, K.; Siemiarczuk, A.; Cowley, D. J.; Baumann, W. *Nouv. J. Chim.* **1979**, 3, 443–454.
- (6) Zachariasse, K. A.; von der Haar, T.; Hebecker, A.; Leinhos, U.; Kühnle, W. *Pure Appl. Chem.* **1993**, 65, 1745–1750.
- (7) Zachariasse, K. A.; Druzhinin, S. I.; Kovalenko, S. A.; Senyushkina, T. *J. Chem. Phys.* **2009**, 131, 224313.
- (8) Gustavsson, T.; Coto, P. B.; Serrano-Andrés, L.; Fujiwara, T.; Lim, E. C. *J. Chem. Phys.* **2009**, 131, 031101.
- (9) Coto, P. B.; Serrano-Andrés, L.; Gustavsson, T.; Fujiwara, T.; Lim, E. C. *Phys. Chem. Chem. Phys.* **2011**, 13, 15182–15188.
- (10) Galván, I. F.; Martín, M. E.; Aguilar, M. A. *Chem. Phys. Lett.* **2010**, 499, 100–102.

- (11) Kwok, W. M.; Ma, C.; Matousek, P.; Parker, A. W.; Phillips, D.; Toner, W. T.; Towrie, M.; Umapathy, S. *Chem. Phys. Lett.* **2008**, *463*, 289–299.
- (12) Park, M.; Kim, C. H.; Joo, T. *J. Phys. Chem. A* **2013**, *117*, 370–377.
- (13) Sobolewski, A. L.; Sudholt, W.; Domcke, W. *J. Phys. Chem. A* **1998**, *102*, 2716–2722.
- (14) Sudholt, W.; Sobolewski, A. L.; Domcke, W. *Chem. Phys.* **1999**, *240*, 9–18.
- (15) Hättig, C.; Hellweg, A.; Köhn, A. *J. Am. Chem. Soc.* **2006**, *128*, 15672–15682.
- (16) Zgierski, M. Z.; Fujiwara, T.; Lim, E. C. *Chem. Phys. Lett.* **2008**, *463*, 289–299.
- (17) Lee, J.-K.; Fujiwara, T.; Kofron, W. G.; Zgierski, M. Z.; Lim, E. C. *J. Chem. Phys.* **2008**, *128*, 164512.
- (18) Pérez Salgado, F.; Herbich, J.; Kunst, A. G. M.; Rettschnick, R. P. H. *J. Phys. Chem. A* **1999**, *103*, 3184–3192.
- (19) Fuß, W.; Pushpa, K. K.; Rettig, W.; Schmid, W. E.; Trushin, S. A. *Photochem. Photobiol. Sci.* **2002**, *1*, 255–262.
- (20) Trushin, S. A.; Yatsushashi, T.; Fuß, W.; Schmid, W. E. *Chem. Phys. Lett.* **2003**, *376*, 282–291.
- (21) Fuß, W.; Schmid, W. E.; Pushpa, K. K.; Trushin, S. A.; Yatsushashi, T. *Phys. Chem. Chem. Phys.* **2007**, *9*, 1151–1169.
- (22) Parusel, A. B. J.; Köhler, G. *J. Phys. Chem. A* **1999**, *103*, 4056–4064.
- (23) Köhn, A.; Hättig, C. *J. Am. Chem. Soc.* **2004**, *126*, 7399–7410.
- (24) Gómez, I.; Reguero, M.; Boggio-Pasqua, M.; Robb, M. A. *J. Am. Chem. Soc.* **2005**, *127*, 7119–7129.
- (25) Sobolewski, A. L.; Domcke, W. *Chem. Phys. Lett.* **1996**, *259*, 119–127.
- (26) Amatatsu, Y. *J. Phys. Chem. A* **2005**, *109*, 7225–7235.
- (27) Xu, X.; Cao, Z.; Zhang, Q. *J. Chem. Phys.* **2005**, *122*, 194305.
- (28) Schenter, G. K.; Duke, C. B. *Chem. Phys. Lett.* **1991**, *176*, 563–570.
- (29) Fonseca, T.; Kim, H. J.; Hynes, J. T. *J. Photochem. Photobiol., A* **1994**, *82*, 67–79.
- (30) Kim, H. J.; Hynes, J. T. *J. Photochem. Photobiol., A* **1997**, *105*, 337–343.
- (31) Hayashi, S.; Ando, K.; Kato, S. *J. Phys. Chem.* **1995**, *99*, 955–964.
- (32) Sudholt, W.; Staib, A.; Sobolewski, A. L.; Domcke, W. *Phys. Chem. Chem. Phys.* **2000**, *2*, 4341–4353.
- (33) Dorairaj, S.; Kim, H. J. *J. Phys. Chem. A* **2002**, *106*, 2322–2327.
- (34) Appel, H.; Di Ventra, M. *Phys. Rev. B* **2009**, *80*, 212303 arXiv:0908.2411 [cond-mat.mtrl-sci].
- (35) Okoshi, M.; Nakai, H. *J. Comput. Chem.* **2014**, *35*, 1473–1480.
- (36) Tully, J. C.; Preston, R. K. *J. Chem. Phys.* **1971**, *55*, 562–572.
- (37) Doltsinis, N. L.; Marx, D. *J. Theor. Comput. Chem.* **2002**, *1*, 319–349.
- (38) Trofimov, A. B.; Schirmer, J. *J. Phys. B: At., Mol. Opt. Phys.* **1995**, *28*, 2299–2324.
- (39) Tully, J. C. *J. Chem. Phys.* **1990**, *93*, 1061–1071.
- (40) Hättig, C. Structure Optimizations for Excited States with Correlated Second-Order Methods: CC2 and ADC(2). In *Advances in Quantum Chemistry*; Jensen, H. J. Å., Ed.; Academic Press: New York, 2005; Vol. 50; pp 37–60.
- (41) Köhn, A.; Tajti, A. *J. Chem. Phys.* **2007**, *127*, 044105.
- (42) Plasser, F.; Crespo-Otero, R.; Pederzoli, M.; Pittner, J.; Lischka, H.; Barbatti, M. *J. Chem. Theory Comput.* **2014**, *10*, 1395–1405.
- (43) Haase, F.; Ahlrichs, R. *J. Comput. Chem.* **1993**, *14*, 907–912.
- (44) Weigend, F.; Häser, M. *Theor. Chem. Acc.* **1997**, *97*, 331–340.
- (45) Hättig, C.; Weigend, F. *J. Chem. Phys.* **2000**, *113*, 5154–5161.
- (46) Köhn, A.; Hättig, C. *J. Chem. Phys.* **2003**, *119*, 5021–5036.
- (47) TURBOMOLE V6.3.1 2010, a development of University of Karlsruhe and Forschungszentrum Karlsruhe GmbH, 1989–2007, TURBOMOLE GmbH, since 2007. Available from <http://www.turbomole.com> (accessed Jan 20, 2015).
- (48) Dunning, T. H., Jr. *J. Chem. Phys.* **1989**, *90*, 1007–1023.
- (49) Weigend, F.; Köhn, A.; Hättig, C. *J. Chem. Phys.* **2002**, *116*, 3175–3183.
- (50) Barbatti, M.; Granucci, G.; Persico, M.; Ruckebauer, M.; Vazdar, M.; Eckert-Maksic, M.; Lischka, H. *J. Photochem. Photobiol., A* **2007**, *190*, 228–240.
- (51) Barbatti, M.; Ruckebauer, M.; Plasser, F.; Pittner, J.; Granucci, G.; Persico, M.; Lischka, H. *Wiley Interdiscip. Rev.: Comput. Mol. Sci.* **2014**, *4*, 26–33.
- (52) Hammes-Schiffer, S.; Tully, J. C. *J. Chem. Phys.* **1993**, *101*, 4657–4667.
- (53) Butcher, J. J. *Assoc. Comput. Mach.* **1965**, *12*, 124–135.
- (54) Hutter, J.; Marx, D. *Ab Initio Molecular Dynamics: Basic Theory and Advanced Methods*; Cambridge University Press: Cambridge, United Kingdom, 2009; pp 22–24.
- (55) Stanton, J. F.; Bartlett, R. J. *J. Chem. Phys.* **1993**, *98*, 7029–7039.
- (56) Stanton, J. F.; Gauss, J.; Harding, M. E.; Szalay, P. G. with contributions from A. A. Auer, R. J. Bartlett, U. Benedikt, C. Berger, D. E. Bernholdt, Y. J. Bomble, L. Cheng, O. Christiansen, M. Heckert, O. Heun, C. Huber, T.-C. Jagau, D. Jonsson, J. Jusélius, K. Klein, W. J. Lauderdale, D. A. Matthews, T. Metzroth, L. A. Müick, D. P. O'Neill, D. R. Price, E. Prochnow, C. Puzzarini, K. Ruud, F. Schiffmann, W. Schwalbach, C. Simmons, S. Stopkowicz, A. Tajti, J. Vázquez, F. Wang, J. D. Watts and the integral packages MOLECULE (J. Almlöf and P. R. Taylor), PROPS (P. R. Taylor), ABACUS (T. Helgaker, H. J. Aa. Jensen, P. Jørgensen, and J. Olsen), and ECP routines by A. V. Mitin and C. van Wüllen. For the current version, see <http://www.cfour.de> (accessed Jan 20, 2015).
- (57) Harding, M. E.; Metzroth, T.; Gauss, J.; Auer, A. A. *J. Chem. Theory Comput.* **2008**, *4*, 64–74.
- (58) Tajti, A.; Szalay, P. G. *J. Chem. Phys.* **2009**, *131*, 124104.
- (59) Parusel, A. B. *J. Phys. Chem. Chem. Phys.* **2000**, *2*, 5545–5552.
- (60) Christiansen, O.; Koch, H.; Jørgensen, P. *J. Chem. Phys.* **1996**, *105*, 1451–1459.
- (61) Druzhinin, S. I.; Demeter, A.; Galievsky, V. A.; Yoshihara, T.; Zacharias, K. A. *J. Phys. Chem. A* **2003**, *107*, 8075–8085.
- (62) Techert, S.; Schotte, F.; Wulff, M. *Phys. Rev. Lett.* **2001**, *86*, 2030–2033.